Z. Phys. B 95, 87–93 (1994)

ZEITSCHRIFT
FÜR PHYSIK B

Dynamic spin and charge susceptibilities in the $t-J$ model

M. Deeg[1], **H. Fehske**[1], **S. Körner**[2], **S. Trimper**[2], **D. Ihle**[3]

[1] Physikalisches Institut, Universität Bayreuth, D-95440 Bayreuth, Germany
[2] Fachbereich Physik, Martin-Luther-Universität Halle, D-06108 Halle, Germany
[3] Fachbereich Physik, Universität Leipzig, D-04109 Leipzig, Germany

Received: 28 December 1993

Abstract. Based on the spin-rotation-invariant formulation of the Kotliar Ruckenstein slave-boson representation, the paramagnetic spin and charge susceptibilities in the $t-J$ model are calculated. Analyzing the static spin susceptibility, the instability of the paraphase towards incommensurate magnetic order is in agreement, with the saddle-point phase diagram recently obtained by some of the authors. The spin dynamics at arbitrary frequencies, wave vectors and band fillings is calculated, where the Fermi-surface and correlation effects are studied. The magnetic instability region is investigated with respect to the formation of a collective spin-fluctuation mode. Near the transition point, a kinetic gap and a sharp peak in the spectral weight ((1,0) paramagnon) are obtained.

PACS: 71.28.+d; 71.45.−d; 71.45.Gm; 75.10.b

1. Introduction

Recently, the unusal magnetic properties in the normal state of high-T_c superconductors (e.g. pseudogap in the spectral weight of the dynamic spin susceptibility of $YBa_2Cu_3O_{6+x}$ for $T_c < T < T_m$ [1, 2]) have attracted increasing attention. The antiferromagnetic spin correlations observed in neutron scattering [1] and NMR [2, 3] experiments are believed to be due to a strong Coulomb repulsion within the Cu 3d orbitals in the CuO_2 planes. To describe the spin dynamics in the metallic state, effective one-band correlation models on a square lattice are a good starting point; besides the Hubbard model, the t-J model is frequently used.

The hithero existing theories of the dynamic spin susceptibility in the t-J model make use of diagrammatic [4] and projection techniques [5], and of the slave-boson (SB) method in the spinon-holon picture [6] combined with the RPA [7] and the self consistent renormalization scheme [8].

In contrast to the Zou-Anderson SB method [6], the SB technique by Kotliar and Ruckenstein for the Hubbard model [9] and the spin-rotation-invariant extension of this theory (SRI SB) [10] have the advantage of treating spin and charge degrees of freedom on an equal footing in the coherent-state path integral. Within the SRI SB technique for the Hubbard model, the ground-state phase diagram in the saddle-point approximation (including spiral magnetic order [11]) and the dynamic response functions (spin and charge susceptibilities), obtained by the one-loop expansion around the paramagnetic saddle point [12], were calculated. In this approach, the instability of the paramagnetic state towards incommensurate magnetic order was investigated by means of the static susceptibility [13].

For an adequate SB description of the magnetic properties and the spin dynamics in the t-J model, in particular for a correct treatment of the antiferromagnetic exchange coupling, one has to use the SRI SB approach. In a recent paper (hereafter referred to as I), Deeg et al. [14] have calculated the magnetic ground-state phase diagram of the t-J model within the SRI SB saddle-point approximation. The phase diagram in the J-δ plane (doping $\delta = 1 - n$), which is shown in Fig. 1, includes paramagnetic (PM), ferromagnetic (FM), antiferromagnetic (AFM), incommensurate (1, 1)-spiral [$\mathbf{Q} = (Q, Q)$] and (1, 0)-spiral [$\mathbf{Q} = (Q, \pi)$] (degenerate, in some region, with the $(0, \pi)$ state), as well as phase-separated states.

Starting from the results obtained in I, the aim of this paper is to investigate the spin and charge fluctuations in the paramagnetic region of the t-J model. To this end, we calculate the wave-vector and frequency-dependent spin and charge susceptibilities within the SRI SB approach. In particular, we are interested in the description of collective spin-fluctuation modes.

The paper is organized as follows. In Sect. 2 the functional integral representation of the partition function in the SRI SB scheme is given and, following the lines indicated by Li et al. [12] for the Hubbard model, analytic expressions for the dynamic response functions at the paramagnetic saddle point are derived. In Sect. 3 numerical results for the dynamic spin susceptibility are presented and discussed. The instability of the paraphase

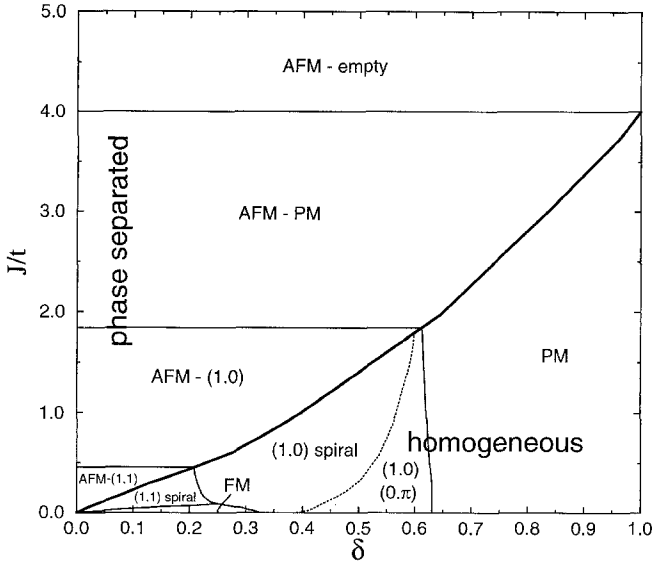

Fig. 1. SRI SB ground-state phase diagram of the *t-J* model taken from I.

against magnetic order is investigated, and particular attention is paid to the frequency dependence and the spin-fluctuation spectral weight. A short summary of our investigations can be found in Sect. 4.

2. Response functions in the SRI SB approach

The *t-J* model is defined by the Hamiltonian

$$\mathscr{H}_{t-J} = -t \sum_{\langle ij\rangle,\sigma} (\tilde{c}^{\dagger}_{i\sigma}\tilde{c}_{j\sigma} + \text{H.c.}) + J \sum_{\langle ij\rangle} \left(\mathbf{S}_i \cdot \mathbf{S}_j - \frac{n_i n_j}{4}\right), \tag{1}$$

with $\mathbf{S}_i = \frac{1}{2}\sum_{\sigma\sigma'} \tilde{c}^{\dagger}_{i\sigma}\tau_{\sigma\sigma'}\tilde{c}_{i\sigma'}$, $n_i = n_{i\uparrow} + n_{i\downarrow}$, and $n_{i\sigma} = \tilde{c}^{\dagger}_{i\sigma}\tilde{c}_{i\sigma}$. The electron annihilation (creation) operator $\tilde{c}^{(\dagger)}_{i\sigma} = c^{(\dagger)}_{i\sigma}(1-n_{i-\sigma})$ acts in a projected Hilbert space without double occupancy. J measures the antiferromagnetic exchange interaction, and t is the transfer amplitude on a square lattice. Following [15, I] the Hilbert space is enlarged by introducing the auxiliary boson fields $e^{(\dagger)}_i$ related to empty sites and the matrix operators $\underline{p}^{(\dagger)}_i$ related to single occupied sites with spin-projection σ according to

$$|0\rangle = e^{\dagger}|\text{vac}\rangle \tag{2}$$

$$|\sigma\rangle = \sum_{\rho} f^{\dagger}_{\rho} p^{\dagger}_{\rho\sigma}|\text{vac}\rangle . \tag{3}$$

Here, the pseudofermions $f^{\dagger}_{\rho}$ are components of a spinor, i.e. the state $|\sigma\rangle$ transforms as a spinor in this representation, and hence the spin-rotation-invariance is ensured. The matrix $\underline{p}^{(\dagger)}_i$ is expressed in terms of the scalar field p_o and the three-component vector field $\mathbf{p} = (p_x, p_y, p_z)$ as

$$\underline{p}^{(\dagger)} = \tfrac{1}{2}\sum_{\mu} \underline{\tau}_{\mu} p^{(\dagger)}_{\mu} . \tag{4}$$

The operators $p^{(\dagger)}_{\mu}$ $(\mu = 0, x, y, z)$ satisfy bosonic commutation rules. To exclude unphysical states occurring in the extended Hilbert space, a set of local constraints has to be fulfilled:

$$C^{(1)} = e^{\dagger}e + \sum_{\mu} p^{\dagger}_{\mu} p_{\mu} - 1 = 0$$

(completeness), (5)

$$C^{(2)}_{\bar{\rho}\rho} = f^{\dagger}_{\rho} f_{\bar{\rho}} - 2\sum_{\rho'} p^{\dagger}_{\bar{\rho}\rho'} p_{\rho'\rho} = 0$$

(SB correspondence). (6)

The electron annihilation operator is transformed due to

$$\tilde{c}_{i\sigma} = \sum_{\rho} z_{i\sigma\rho} f_{i\rho} \tag{7}$$

with

$$\underline{z} = \underline{L} e^{\dagger} \underline{M} \underline{p} \underline{R}, \quad \underline{R} = [(1 - e^{\dagger}e)\underline{1} - 2\underline{\tilde{p}}^{\dagger}\underline{\tilde{p}}]^{-1/2},$$

$$\underline{L} = [\underline{1} - 2\underline{p}^{\dagger}\underline{p}]^{-1/2}, \quad M = [1 + e^{\dagger}e + 2\,\mathrm{Tr}\,\underline{p}^{\dagger}\underline{p}]^{1/2},$$

and

$$\tilde{p}^{(\dagger)}_{\rho\rho'} := \rho\rho' p^{(\dagger)}_{-\rho'-\rho},$$

choosen according to [15]. Furthermore, the spin and the particle number operator have to be bosonized:

$$n_i(p_{i\mu}) = 2\,\mathrm{Tr}\,\underline{p}^{\dagger}_i \underline{p}_i , \tag{8}$$

$$\mathbf{S}_i(p_{i\mu}) = \mathrm{Tr}\,\underline{p}^{\dagger}_i \underline{\tau}\,\underline{p}_i . \tag{9}$$

The local constraints are enforced by time independent Lagrange multipliers $\lambda^{(1)}_i$ and $\lambda^{(2)}_{i\mu}$, i.e. the Hamiltonian of the *t-J* model in terms of the slave boson operators $\mathscr{H}^{SB}_{t-J}$ has to be replaced by

$$\mathscr{H}^{SB}_{t-J} + \sum_i (C^{(1)}_i \lambda^{(1)}_i + \mathrm{Tr}\,\underline{C}^{(2)}_i \underline{\lambda}^{(2)}_i),$$

with

$$\underline{\lambda}^{(2)}_i = \sum_{\mu} \underline{\tau}_{\mu} \lambda^{(2)}_{i\mu} .$$

Now the partition function may be expressed using a coherent-states path integral over complex bosonic and pseudofermionic Grassmann fields. The resulting Lagrangian is invariant under a local $SU(2) \otimes U(1)$ gauge transformation which can be used to remove the phases of *all* the boson fields (see I) and changes the Lagrange multipliers to time-dependent ones. In the radial gauge, we are able to integrate out the fermionic degrees of freedom. Then we obtain an exact representation of the partition function

$$\mathscr{Z} = \int \mathscr{D}[\Phi^*, \Phi] e^{-\mathscr{S}_{\text{eff}}} \tag{10}$$

in terms of the Bose fields

$$\Phi_i(\tau) = (\{\phi_{i\alpha}(\tau)\})$$

$$= (e_i, p_{io}, \lambda^{(2)}_{io}, \lambda^{(1)}_i; p_{ix}, \lambda^{(2)}_{ix}; p_{iy}, \lambda^{(2)}_{iy}; p_{iz}, \lambda^{(2)}_{iz}),$$

$$\alpha = 1 \ldots 10 . \tag{11}$$

The bosonic part of the effective action $\mathscr{S}_{\text{eff}}=\mathscr{S}_{\text{eff}}^{B}+\mathscr{S}_{\text{eff}}^{F}$ is given by

$$\mathscr{S}_{\text{eff}}^{B}=\int_0^\beta \mathrm{d}\tau\left\{\sum_i\left[\lambda_i^{(1)}e_i^2+\sum_\mu(\lambda_i^{(1)}-\lambda_{io}^{(2)})p_{i\mu}^2 -2p_{io}\mathbf{p}_i\cdot\boldsymbol{\lambda}_i^{(2)}-\lambda_i^{(1)}\right] +J\sum_{\langle ij\rangle}[p_{io}\mathbf{p}_i\cdot\mathbf{p}_j p_{jo}-\tfrac{1}{4}(p_{io}^2+\mathbf{p}_i^2)(p_{jo}^2+\mathbf{p}_j^2)]\right\}. \tag{12}$$

The fermionic part reads

$$\mathscr{S}_{\text{eff}}^{F}=\mathrm{Tr}_{ij,\tau\tau',\rho\rho'}\ln\{-G_{ij,\rho\rho'}^{-1}(\tau,\tau')\} \tag{13}$$

with

$$G_{ij,\rho\rho'}^{-1}(\tau,\tau')=[(-\partial_\tau+\mu-\lambda_{io}^{(2)})\delta_{\rho\rho'}-\boldsymbol{\lambda}_i^{(2)}\cdot\boldsymbol{\tau}_{\rho\rho'}] \times\delta_{ij}\delta(\tau-\tau')+t(\underline{z}_i^{\dagger}\underline{z}_j)_{\rho\rho',\tau\tau'}(1-\delta_{ij}). \tag{14}$$

To proceed, we apply (i) the static approximation for the ten real boson fields at the uniform paramagnetic saddle point and (ii) we only take into account the Gaussian fluctuations around the paramagnetic saddle point [12]. Introducing the notations $q=(\mathbf{q},\omega_m)$, $R_i=(\mathbf{R}_i,\tau)$, $\mathscr{N}=\beta N$, and $\sum_{R_i}=\sum_i\int_0^\beta \mathrm{d}\tau$, where ω_m are the Bose- or the Fermi-Matsubara frequencies, the effective action $\mathscr{S}_{\text{eff}}$ can be written as

$$\mathscr{S}_{\text{eff}}=\bar{\mathscr{S}}+\sum_{\substack{q\\ \alpha,\beta}}\varphi_\alpha(-q)\mathscr{S}_{\alpha\beta}(q)\varphi_\beta(q). \tag{15}$$

To find the last expression we have decomposed the field Φ_i in the saddle-point part $\bar{\Phi}$ and the correction part φ_i, $\Phi_i=\bar{\Phi}+\varphi_i$, where

$$\bar{\Phi}=(e,p_o,\lambda_o^{(2)},\lambda^{(1)};0,0;0,0;0,0),\qquad \varphi_i=(\{\varphi_{i\alpha}\})=(\{\delta\phi_{i\alpha}\}). \tag{16}$$

The paramagnetic saddle-point solution, at $T=0$, is given by

$$e^2=\delta, \tag{17}$$

$$p_o^2=1-\delta, \tag{18}$$

$$\lambda^{(1)}=-\frac{2+3\delta-\delta^2}{1-\delta^2}\tilde{\varepsilon}(0), \tag{19}$$

$$\lambda_o^{(2)}=-\frac{2}{(1+\delta)^2}\tilde{\varepsilon}(0)-(1-\delta)J, \tag{20}$$

where we have used the notation

$$\tilde{\varepsilon}(\mathbf{q})=\frac{2}{N}\sum_{\mathbf{k}}\varepsilon_{\mathbf{k}-\mathbf{q}}\theta(\mu-E_{\mathbf{k}}), \tag{21}$$

$$\varepsilon_{\mathbf{k}}=-2t(\cos k_x+\cos k_y). \tag{22}$$

Here the quasiparticle energy is

$$E_{\mathbf{k}}=z^2\varepsilon_{\mathbf{k}}+\lambda_o^{(2)} \tag{23}$$

with $z^2=2\delta/(1+\delta)$. The chemical potential μ is determined for a given hole density $\delta=1-n$ from $n=\frac{2}{N}\sum_{\mathbf{k}}\theta(\mu-E_{\mathbf{k}})$. The (paramagnetic) mean-field free energy per site then simply becomes

$$\frac{\bar{\mathscr{S}}}{\mathscr{N}}=z^2\tilde{\varepsilon}(0)-\tfrac{1}{2}J(1-\delta)^2. \tag{24}$$

The fluctuation matrix $\mathscr{S}_{\alpha\beta}$ can be calculated according to

$$\mathscr{S}_{\alpha\beta}(q,q')=\mathscr{S}_{\alpha\beta}(q)\delta(q+q') =\frac{1}{2\mathscr{N}}\sum_{R_i,R_j}e^{-\mathrm{i}qR_i}\frac{\partial^2\mathscr{S}}{\partial\phi_{i\alpha}\,\partial\phi_{j\beta}}\bigg|_{\substack{\Phi_i=\Phi_j=\bar{\Phi}\\ \delta(\tau-\tau')}}e^{-\mathrm{i}q'R_j}. \tag{25}$$

Following [12] we now define the spin and charge susceptibilities by the relations

$$\chi_s(q)=\sum_{\sigma\sigma'}\sigma\sigma'\langle\delta n_\sigma(-q)\delta n_{\sigma'}(q)\rangle, \tag{26}$$

$$\chi_c(q)=\sum_{\sigma\sigma'}\langle\delta n_\sigma(-q)\delta n_{\sigma'}(q)\rangle. \tag{27}$$

In terms of the SB fields, (26) and (27) are expressed as

$$\chi_s(q)=4p_o^2\langle\delta p_z(-q)\delta p_z(q)\rangle \tag{28}$$

$$\chi_c(q)=4e^2\langle\delta e(-q)\delta e(q)\rangle, \tag{29}$$

respectively. Here the correlation functions are related to the inverse fluctuation matrix by

$$\langle\varphi_\alpha(-q)\varphi_\beta(q)\rangle=\tfrac{1}{2}(\mathscr{S}^{-1})_{\alpha\beta}. \tag{30}$$

It is easy to see that at the PM saddle point the fluctuation matrix $\mathscr{S}$ decomposes into a 4×4 matrix denoted by $\underline{A}$ (connected to charge fluctuations) and three identical 2×2 matrices denoted by $\underline{B}$ (connected to spin fluctuations), respectively. Whereas the $\underline{A}$ matrix is built up by the elements $(\delta e_i,\delta p_{io},\delta\lambda_{io}^{(2)},\delta\lambda_i^{(1)})$, the $\underline{B}$ matrix is based, e.g., upon the elements $(\delta p_{ix},\delta\lambda_{ix}^{(2)})$. Accordingly, the spin and the charge susceptibility can be written in the form

$$\chi_s(q)=2p_o^2(\mathscr{S}^{-1})_{55}=2p_o^2\frac{\mathscr{S}_{66}}{\det\underline{B}}, \tag{31}$$

$$\chi_c(q)=2e^2(\mathscr{S}^{-1})_{11}=-2e^2p_o^2\frac{\mathscr{S}_{33}}{\det\underline{A}}. \tag{32}$$

From here we may derive the following expression for both the spin and the charge susceptibility:

$$\chi_{s,c}(q)=\frac{\chi_o(q)}{1+C_o(\mathbf{q})\chi_o(q)+C_1\chi_1(q)+\frac{C_1^2}{4}\{\chi_1^2(q)-\chi_o(q)\chi_2(q)\}}, \tag{33}$$

where

$$C_l=\begin{cases}A_l, & \text{for } \chi_s\\ B_l, & \text{for } \chi_c\end{cases} \tag{34}$$

with

$$A_o(\mathbf{q})=\frac{\delta}{(1+\delta)^3}\{\tilde{\varepsilon}(\mathbf{q})+3\tilde{\varepsilon}(0)\}+\tfrac{1}{2}J(\mathbf{q}), \tag{35}$$

$$A_1=\frac{2\delta}{(1+\delta)^2}, \tag{36}$$

$$B_o(\mathbf{q})=\frac{1}{\delta(1+\delta)^3}\{\tilde{\varepsilon}(\mathbf{q})-(4\delta+1)\tilde{\varepsilon}(0)\}-\tfrac{1}{2}J(\mathbf{q}), \tag{37}$$

$$B_1=-\frac{2}{(1+\delta)^2}. \tag{38}$$

In the last equations we have used the following abbreviations:

$$J(\mathbf{q})=J(\cos q_x+\cos q_y), \tag{40}$$

$$\chi_n(q)=-\frac{2}{\mathcal{N}}\sum_k(\varepsilon_{\mathbf{k}}+\varepsilon_{\mathbf{k}+\mathbf{q}})^n G(k)G(k+q),\quad n=0,1,2, \tag{41}$$

$$G(k)=\frac{1}{i\omega_n-E_{\mathbf{k}}+\mu}. \tag{42}$$

The response functions (33) exhibit a similar analytical structure as for the Hubbard model [12]. However, for the t-J model the coefficients C_l can be given in a much simpler and explicit form.

3. Numerical results and discussion

We have numerically evaluated the wave-vector and frequency-dependent spin susceptibility $\chi_s(\mathbf{q},\omega)=\chi_s'(\mathbf{q},\omega)+i\chi_s''(\mathbf{q},\omega)$ given by (33) for different band fillings and parameters J/t (the realisitic value $J/t=0.4$ is taken from I and yields a good agreement of the spiral order vector with neutron scattering data). Let us first consider the static susceptibility $\chi_s(\mathbf{q})$, where we are primarily interested in the instability line of the paraphase against magnetic structures (determined from the poles of $\chi_s(\mathbf{q})$ in $\mathbf{q}$ space), as suggested from the phase diagram (Fig. 1).

In Fig. 2 some representative results for $\chi_s(\mathbf{q})$ (a, c, e) and the response functions $\chi_n(\mathbf{q})$ (b, d, f) along the high-symmetry directions are shown. For low electron densities ($\delta=0.75$, Fig. 2a, b), the SB renormalized quasi-particle band structure has a nearly circular Fermi surface (FS). In the small $\mathbf{q}$ region, the weak dependence on $\mathbf{q}$ of χ_0 and χ_s (for small J/t) is in accord with the flatness of the response function $\chi_0(\mathbf{q})$ for the two-dimensional parabolic band dispersion up to the Kohn anomaly at $2k_F$ [16]. Note that for small wave-numbers, the enhancement of χ_s with respect to χ_0 decreases with increasing J. The Kohn anomalies at $\mathbf{Q}_K=2\mathbf{k}_F$ (joining two points on the FS with antiparallel Fermi velocities) are reflected in maxima of χ_0 and χ_s. In the $(0,q)$ and (q,q) directions the anomalies occur at $\mathbf{Q}_{K_1}=(0,2.56)$ and $\mathbf{Q}_{K_2}=(1.74,1.74)$, respectively, where $\mathbf{Q}_{K_1}|/|\mathbf{Q}_{K_2}|=1.04$ expresses the very small FS anisotropy (for the square FS in the $\delta=0$ case, we have $|\mathbf{Q}_{K_1}|/|\mathbf{Q}_{K_2}|=\sqrt{2}$). Let us point out that for $J/t=4$, at $\delta_c^{(1,1)}=0.69$ the paraphase is unstable against the (1, 1) spiral state (see the sharp structure in χ_s at $\mathbf{Q}_{K_2}=(1.85,1.85)$. However, this transition is not realized since the AFM-PM phase separated state is lower in energy (cf. Fig. 1). The instability against phase separation cannot be seen in $\chi_s(\mathbf{q})$.

In Fig. 2c and d the results at the critical hole concentration $\delta_c^{(1,0)}=0.6294$ for the second-order PM-$(0,\pi)$ state phase transition (which is nearly independent of J [14], cf. Fig. 1) are depicted. Along the $(0,q)$ direction, the Kohn anomaly of $\chi_n(\mathbf{q})$ occurs at $\mathbf{Q}_{K_1}=(0,\pi)$ which results in a divergence of χ_s at $\mathbf{Q}_{K_1}$. Let us emphasize that this instability is mainly governed by the pronounced $\mathbf{q}$ dependence of the function $\chi_2(\mathbf{q})$ (on the contrary, $\chi_0(\mathbf{q})$ for larger δ is nearly constant in the whole Brillouin zone). Thus the instability line determined from the poles of the paramagnetic spin susceptibility coincides with the phase boundary between the paraphase and the $(0,\pi)$ state calculated in I by the saddle-point solution. This proves the consistency of both approaches. Note that $\mathbf{Q}_{K_2}=(2.1,2.1)$ and $|\mathbf{Q}_{K_1}|/|\mathbf{Q}_{K_2}|=1.06$ expresses the increasing FS anisotropy with decreasing δ. For $J/t=0.4$, the sharp structures in the *paramagnetic* susceptibility $\chi_s(\mathbf{q})$ near $\mathbf{Q}_{K_2}$ reveal that the system has passed the PM-(1, 1)-spiral instability point.

For comparison with the above results and with the spin-fluctuation theory by Tanamoto et al. [7], in Fig. 2e we have plotted $\chi_s(\mathbf{q})$ for $\delta=0.1$ lying far in the instability region (see Figs. 1, 2a, 2c), where magnetically ordered states are realized. At $\delta=0.1$ ("rounded-square" FS), the Kohn anomalies in $\chi_0(\mathbf{q})$ appear at $\mathbf{Q}_{K_1}=(0,2\pi-2k_F)$, where $2k_F=5.4>\pi$ and the y-component is reduced into the first Brillouin zone (umklapp scattering), and at the "pseudo-nesting" vector $\mathbf{Q}_{K_2}=(3.0,3.0)$ $(2k_F/|\mathbf{Q}_{K_2}|=1.27)$ (see Fig. 2f). In addition a sharp incommensurate Kohn peak occurs at $\mathbf{Q}_{K_3}=(\pi-\eta,\pi)$, $\eta\simeq 0.2$. A similar behaviour of $\chi_0(\mathbf{q})$ in the small-doping region was also found in previous RPA-like fluctuation theories for the t-J [7] and Hubbard models (see, e.g., [17, 18]. Whereas in the spinon-holon theory by Tanamoto et al. [7], $\chi_s(\mathbf{q})$ behaves qualitatively similar as $\chi_0(\mathbf{q})$ and the maximum of $\chi_0(\mathbf{q})$ at $\mathbf{Q}_{K_3}$ may give rise to a spiral order for small δ $(0<\eta\ll\pi)$, in our SB approach the situation is quite different. The instability occurs, at much larger values of δ against the $(0,\pi)$ ordered state which is due to the predominant role of $\chi_2(\mathbf{q})$ near $(0,\pi)$.

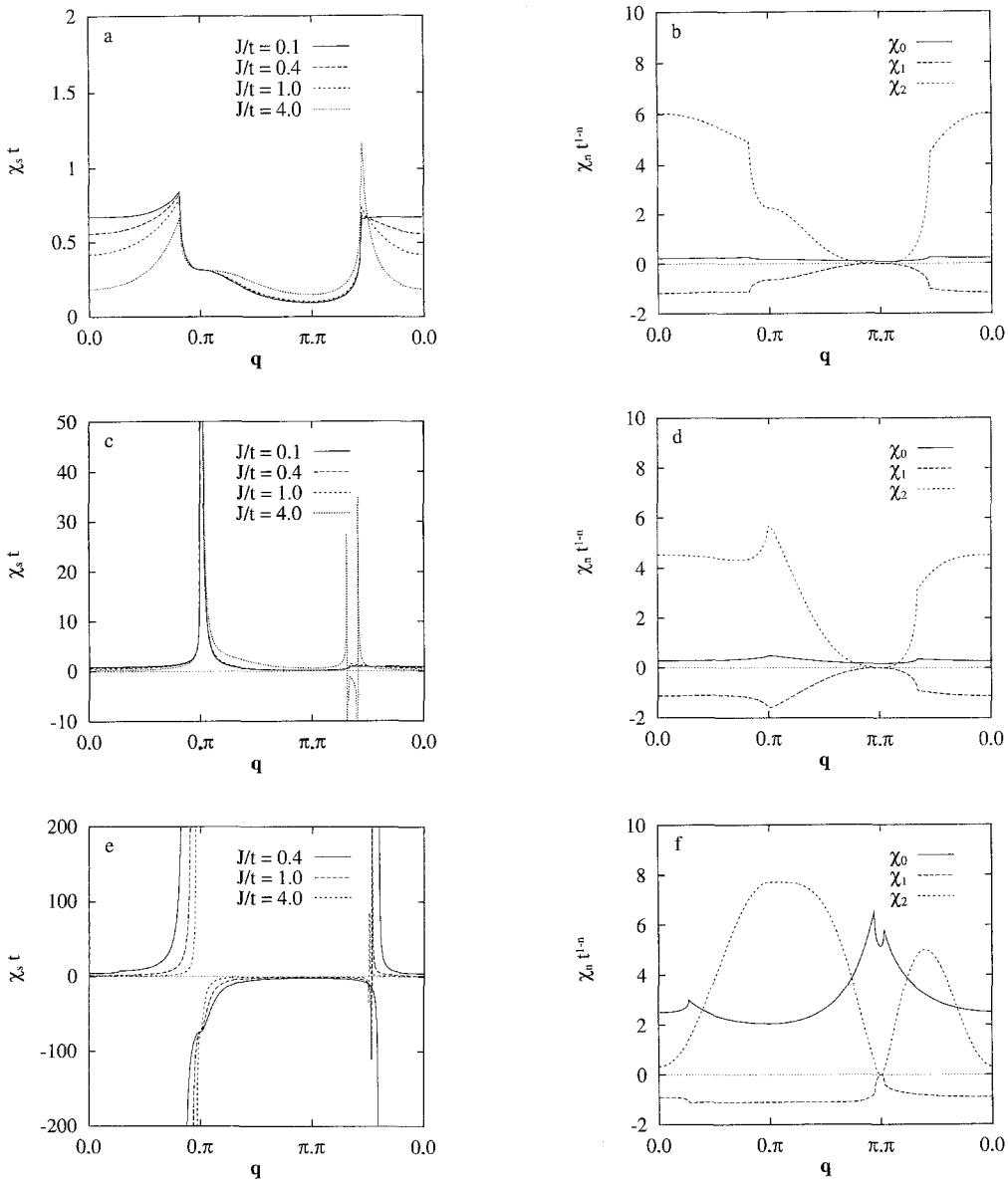

Fig. 2. Static spin susceptibility as function of $\mathbf{q}$ for different band fillings $\delta = 0.75$ **a**, **b**, $\delta_c^{(1,0)} = 0.6294$ **c**, **d** and $\delta = 0.1$ **e**, **f**. For comparison, the corresponding response functions $\chi_n(\mathbf{q})$ **b**, **d**, **f** are shown

To study the spin dynamics, in Fig. 3 the results for $\chi_s'(\mathbf{q}, \omega)$ and $\chi_s''(\mathbf{q}, \omega)$ in the paraphase with $\delta = 0.63$ at fixed $\omega/t = 0.1$ (Fig. 3a, b) and $\omega/t = 0.3$ (Fig. 3c, d) versus $\mathbf{q}$ are shown. For finite frequencies, the sharp Kohn peak in $\chi_s'(\mathbf{q}, \omega = 0)$ at $\mathbf{Q}_{K_1}$ near $(0, \pi)$ is split into two incommensurate maxima. This may be interpreted as follows. The small energy transfer ω/t creates an effective momentum of the particle-hole pairs which slightly deviates from $\mathbf{Q}_{K_1}$ resulting in an incommensurate peak structure of $\chi_s'(\mathbf{q}, \omega)$ (analogous to that found for $\chi_0(\mathbf{q})$ in the case of Fig. 2f). In correspondence with this, the spectral weight $\chi_s''(\mathbf{q}, \omega)$ has a pronounced structure near $(0, \pi)$. The vanishing of χ_s'' in some $\mathbf{q}$ region is also known from the Lindhard function for the free electron gas. With increasing frequency (Fig. 3c, d) the separation between the incommensurate peaks in χ_s' increases and the structure is smeared out (especially, the ratio of the maximum height to the minimum at $(0, \pi)$ decreases). At the same time, the features in χ_s'' near $(0, \pi)$ become less pronounced. For $J/t = 4$, in passing the PM-(1, 0)-state transition point with increasing ω, $\chi_s'(\mathbf{q}, \omega)$ at $\mathbf{q} = \mathbf{Q}_{\max}^{(1,0)}(\omega)$ develops similar structures as for the δ-driven transition at $\omega = 0$ (cf. Fig. 2). The imaginary part reveals a pronounced absorption.

To investigate this transition region in more detail, in Fig. 4 the real (a) and the imaginary (b) part of $\chi_s((0, \pi), \omega)$ are shown as functions of ω for various doping levels $\delta \gtrsim \delta_c^{(1,0)}(\omega = 0)$. Approaching $\delta_c^{(1,0)}(\omega = 0)$ from above, a sharp maximum in χ_s' and χ_s'' develops at $\delta_c^{(1,0)}(\omega_c)$. The pronounced absorption maximum at $\omega_c/t = 0.0112$ describes the excitation of a collective mode ((1, 0)-paramagnon). Note that $\delta_c^{(1,0)}(\omega > 0) \gtrsim \delta_c^{(1,0)}(\omega = 0)$. For $\delta \lesssim \delta_c^{(1,0)}(\omega_c)$, $\chi_s'((0, \pi), \omega)$ exhibits, as function of ω, a similar structure as $\chi_s'(\mathbf{q}, \omega = \text{const.})$ below the transition point (cf. Figs. 2 and 3). If, for a given value of δ, the wave vector

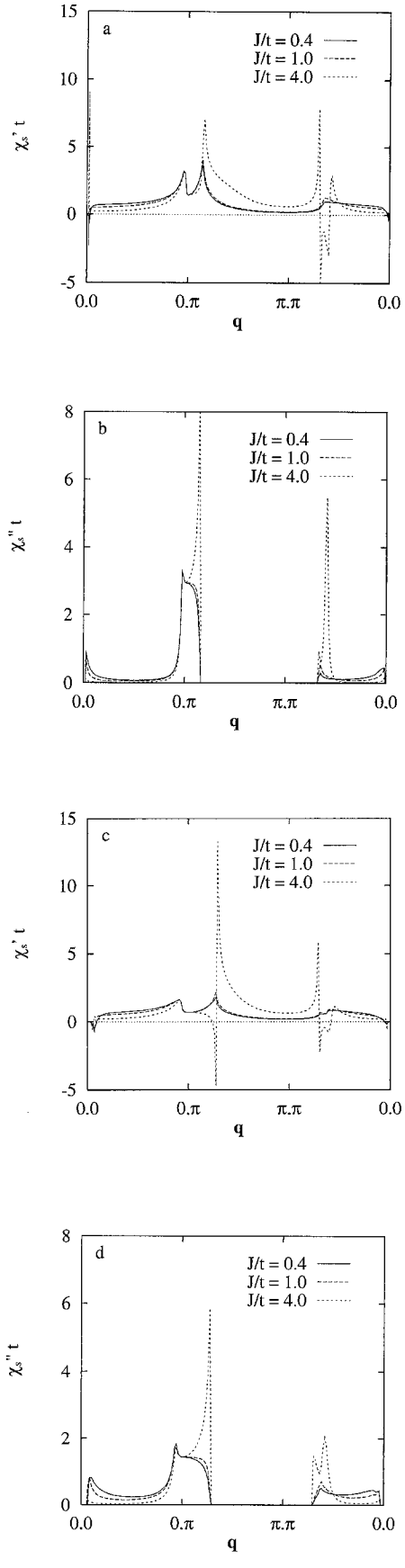

Fig. 3. Real **a**, **c** and imaginary parts **b**, **d** of the dynamic spin susceptibility for $\delta = 0.63$ and $\omega/t = 0.1$ **a**, **b**, 0.3 **c**, **d** as function of **q**

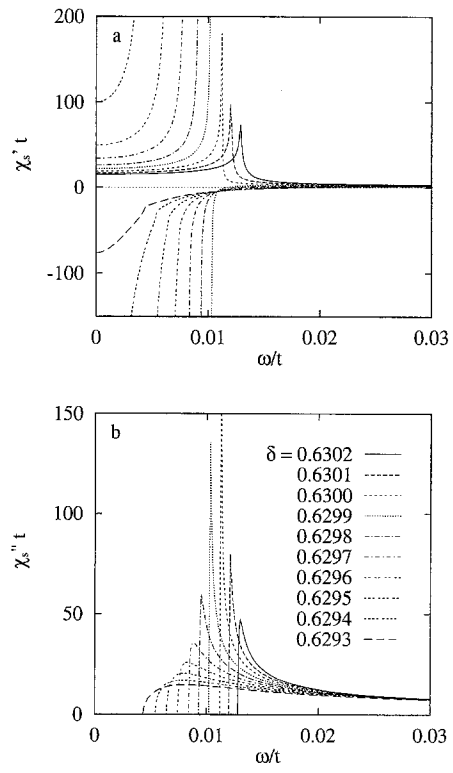

Fig. 4. Frequency dependences of the real **a** and imaginary parts **b** of the spin susceptibility near the PM-$(0, \pi)$ state phase transition for $J/t = 0.4$, $\mathbf{q} = (0, \pi)$ and different fillings near the critical value of $\delta_c^{(1,0)}$. The line style is depicted in **b**

deviates from the Kohn anomaly value, there occurs a kinetic gap in the spectral weight χ_s'' (Fig. 4b; compare the discussion given in [18, 19]). The gap formation may be explained by the excitation of particle-hole pairs with an effective momentum $\mathbf{Q}_{K_1}$ spanning the FS and with a finite spectral weight.

In Fig. 5 the frequency dependences of $\chi_s'(\mathbf{q}, \omega)$ and $\chi_s''(\mathbf{q}, \omega)$ for larger doping ($\delta = 0.75$), $J/t = 0.4$ and at different fixed $\mathbf{q}$ values are shown. They exhibit the characteristic behaviour of response functions (in accordance with the Kramers-Kronig relation), i.e. the zero-crossing of χ_s' near the maximum of χ'''s. At $\mathbf{q} = \mathbf{Q}_{K_1} = (0, 2.56)$, where $\chi_s(\mathbf{q})$ has a maximum (cf. in Fig. 2a), the spectral weight describes the particle-hole continuum. As seen in Fig. 5, the kinetic gap increases with increasing deviation of q_y from the anomaly value.

4. Summary

In this paper we have calculated the two-point dynamic response functions in the t-J model within the SRI SB approach taking into account the Gaussian fluctuations around the paramagnetic saddle point. Our main results are the following:

(i) For the spin and charge susceptibilities, we have derived explicit analytical expressions going beyond the standard RPA form.

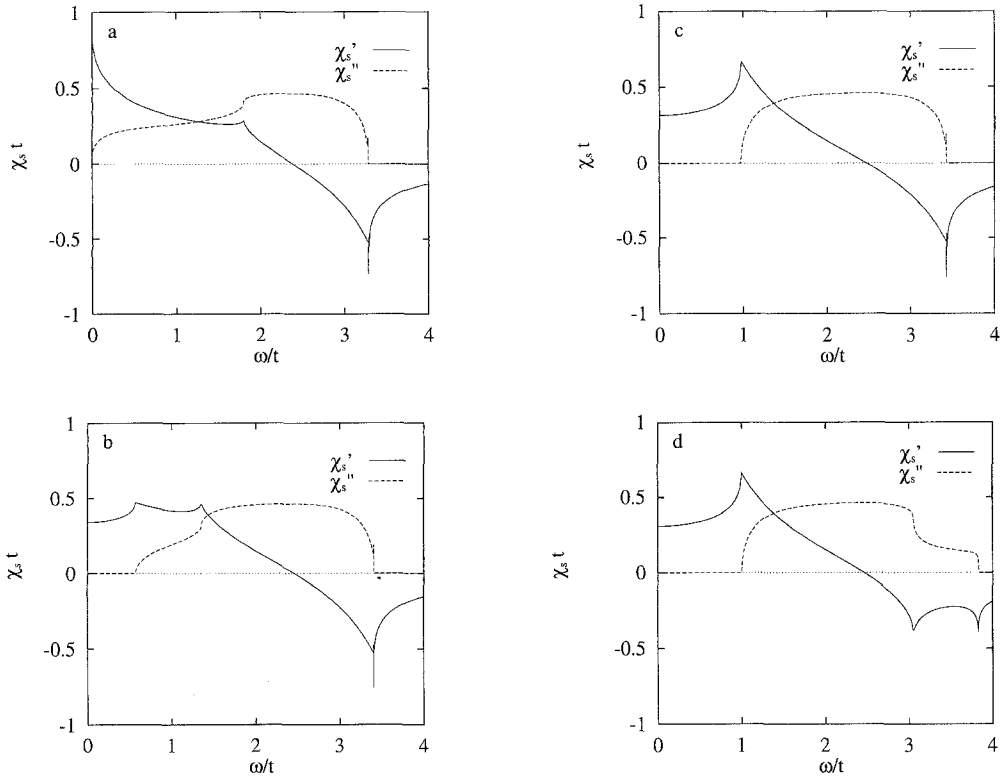

Fig. 5. Frequency dependence of the spin susceptibility for $J/t=0.4$, $\delta=0.75$ and different wave vectors $\mathbf{q}=(0,2.56)$ **a**, $\mathbf{q}=(0,2.9)$ **b**, $\mathbf{q}=(0,\pi)$ **c** and $\mathbf{q}=(0.24,\pi)$ **d**

(ii) We have performed a detailed numerical evaluation of the spin susceptibility for arbitrary frequencies, wave vectors, band fillings and exchange interactions. The static and dynamic susceptibilities are found to be qualitatively affected by the SB-renormalized Fermi-surface geometry.
(iii) The instability line of the paraphase against incommensurate magnetic order, determined by a divergency in the static susceptibility, is in agreement with the phase boundary in the saddle-point phase diagram.
(iv) Near the PM-$(0,\pi)$ state phase transition, we have found a collective spin-fluctuation mode ($(1,0)$ paramagnon), where the spectral weight has a kinetic gap followed by a sharp peak structure.

H.F. acknowledges the support of the NTZ and the hospitality at the University of Leipzig. At Bayreuth, this work was supported in part by SFB 213 (M.D. and D.I.). We also thank H. Büttner for valuable discussions.

References

1. Rossat-Mignod, J., Regnault, L.P., Bourges, P., Vettier, C., Bourlet, P., Henry, J.Y.: Physica B**186–188**, 1 (1993)
2. Horvatic, M., Butaud, B., Segransan, P., Berthier, Y., Berthier, C.: Physica C**166**, 151 (1990)
3. Millis, A.J., Monien, H.: Phys. Rev. B**45**, 3059 (1992)
4. Izyumov, Y.A., Letfulov, B.M.: J. Phys. Condens. Matter **2**, 8905 (1990)
5. Becker, K.W., Muschelknautz, U.: Phys. Rev. B**48**, 13826 (1993)
6. Zou, Z., Anderson, P.W.: Phys. Rev. B**37**, 627 (1988)
7. Tanamoto, T., Kuboki, K., Fukuyama, H.: J. Phys. Soc. Jpn. **60**, 3072 (1991); Tanamoto, T., Kohno, H., Fukuyama, H.: J. Phys. Soc. Jpn. **62**, 717 (1993); ibid. **62**, 1455 (1993)
8. Grempel, R., Lavagna, M.: Solid State Commun. **83**, 595 (1992)
9. Kotliar, G., Ruckenstein, A.E.: Phys. Rev. Lett. **57**, 1362 (1986)
10. Li, T., Wölfle, P., Hirschfeld. P.J.: Phys. Rev. B**40**, 6817 (1989)
11. Frésard, R., Dzierzawa, M., Wölfle, P.: Europhys. Lett. **15**, 325 (1991); Möller, B., Doll, K., Frésard, R.: J. Phys. Cond. Matter **5**, 4847 (1993)
12. Li, T., Sun, Y.S., Wölfle, P.: Z. Phys. B**82**, 369 (1991)
13. Doll, K., Dzierzawa, M., Frésard, R., Wölfle, P.: Z. Phys. B**90**, 297 (1993)
14. Deeg, M., Fehske, H., Büttner, H.: Europhys. Lett. (accepted for publication 1994)
15. Frésard, R., Wölfle, P.: Int. Mod. Phys. B**5&6**, 685 (1992); Erratum ibid. **6**, 3087 (1992)
16. Gabay, M., Béal-Monod, M.T.: Phys. Rev. B**18**, 5033 (1978)
17. Wermbter, S., Tewordt, L.: Phys. Rev. B**43**, 10530 (1991); ibid. **48**, 10514 (1993)
18. Bénard, P., Chen, L., Tremblay, A.-M., S.: Phys. Rev. B**47**, 15217 (1993)
19. Bulut, N., Scalapino, D.J.: (Preprint UCSBTH-90-69)